ELSEVIER

Seminars in ULTRASOUND CT and MRI

Current and Future Applications of Thoracic Dual-Energy CT in Children: Pearls and Pitfalls of Technique and Interpretation

Jordan B. Rapp,[*,†] David M. Biko,[*,†] Christian A. Barrera,[*] Summer L. Kaplan,[*,†] and Hansel J. Otero[*,†]

Dual-energy computer tomography (DECT) technology has experienced rapid growth in recent years, now allowing for the collection of 2 CT data sets and opening the potential for functional data acquisition. Data from a single postcontrast phase are deconstructed and Iodine can be subtracted to create a virtual noncontrast image, or selectively represented as a contrast map that allows for the qualification and quantification of lung perfusion. Virtual monoenergetic images can also be used to reduce beam-hardening artifact from concentrated contrast or metal implants. In children, DECT is of particular interest because it has been shown to be dose neutral in most applications, dose-reducing in multiphase studies, and to increase the contrast to noise ratio in suboptimal studies. We review the basics of acquisition, postprocessing, and thoracic applications of DECT with a focus on pulmonary blood volumes as a surrogate for perfusion imaging. The discussed applications include pulmonary embolism, hypoplastic lung, pulmonary hypertension in bronchopulmonary dysplasia, and pediatric lung masses.
Semin Ultrasound CT MRI 41:433-441

Introduction

Dual-energy computed tomography (DECT) has experience rapid growth in recent years, allowing for the collection of 2 synchronous data sets, displayed as a single mixed image for clinical interpretation.[1,2] However, the acquisition of 2 separate datasets open the potential for functional data in which iodine can be subtracted to create a virtual noncontrast image, or selectively represented as a contrast map. The most commonly discussed applications of DECT in adults include evaluation of pulmonary embolism (PE), renal calculi, and reduction of metal artifact, which are relatively well established with enough published evidence to support its use.[1,3,4] Additional cardiovascular applications in adults include contrast amplification, myocardial perfusion, as well as plaque and thrombus characterization.[1] These applications are based on post processing of DECT data that allows for imaging display (qualification) and quantification of iodinated contrast volumes, a surrogate for perfusion. In children, DECT is of interest because it has been shown to be dose neutral in most applications, dose-reducing in multiphase studies, increase the contrast to noise ratio in suboptimal studies, and allow for protocols with reduced contrast dosing.[1,5,6] Moreover, advanced applications that include DECT-based perfusion could prove useful in the evaluation and prognosis of pediatric-specific conditions including chronic lung disease of prematurity, lung hypoplasia, and uniquely pediatric lung lesions such as sequestration and congenital pulmonary airway malformation. This review describes the basics of acquisition, postprocessing, and clinical applications of DECT-based perfusion in children.

Pearls in imaging acquisition and technique

Scanner types

Dual energy CT technology, though first described in the 1970s, has advanced over the past decade resulting in images

*Children's Hospital of Philadelphia, Department of Radiology, 3401 Civic Center Blvd, Philadelphia, PA.
†University of Pennsylvania, Perelman School of Medicine, Philadelphia, PA.
Address reprint requests to Jordan B. Rapp, MD. Department of Radiology, Children's Hospital of Philadelphia, 3401 Civic center Blvd, Philadelphia, PA 19096. E-mail: rappj@email.chop.edu

https://doi.org/10.1053/j.sult.2020.05.008
0887-2171/

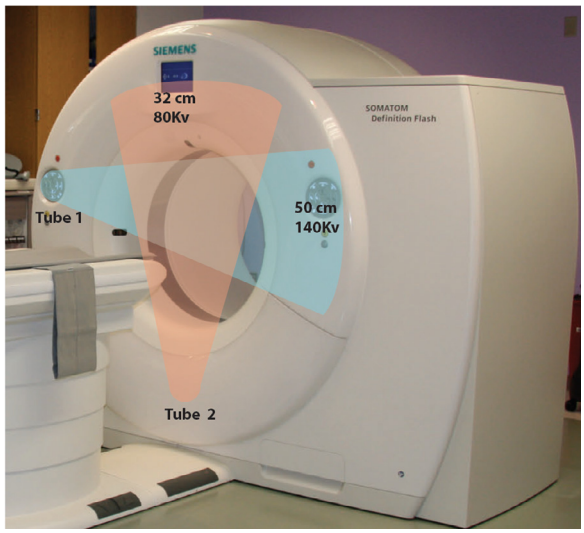

Figure 1 Dual source DECT diagram. The 80 kv source with a smaller 32 cm FOV is located 90° from the 140 kV 50 cm FOV source.

that are not just diagnostic but also functional. Dual energy CT now comes in a variety of flavors including a number of single source options: rapid kilovolt (kV) switching, dual-layer detector, split beam, and temporal scanning with 2 consecutive acquisitions.[1] The alternative is the dual-source option, where 2 energy beams are simultaneous applied at different kV from 2 sources located 90° from each other (Fig. 1). Multiple vendors offer DECT technology; at our institution, DECT scans are performed on a Somatom Definition Flash (Siemens Healthcare, Forchheim, Germany).

Distinct data sets are created, can be interpreted separately or as a composite image

Most typically in the small pediatric patient, 80 kV is used for the low-energy beam, and 140 kV for the high-energy beam. As an alternative in larger patients we utilize a higher low energy of 100 kV, to counterbalanced increased image noise, while maintaining the higher energy at 140 kV; for the purposes of this review we refer to the data sets as 80 kV/140 kV, the more common permutation in the pediatric patient and commonly utilized at our institution.

The acquisition at 80 kV and 140 kV results in 2 data sets which will then be mixed in a 60:40 ratio to form a composite image. This mixed ratio can be adjusted after scanning to create images anywhere between 80 kV and 140 kV with different degree of inclusion of each source set (Fig. 2). Typically, the composite images will be used for interpretation in the same manner as a single-source single-energy CT would.

The principle behind DECT is material decomposition where different energies are used to allow decomposition of specific materials.[2] A single sources DECT scanner can only utilize 2 material decomposition, typically water and iodine.[7]

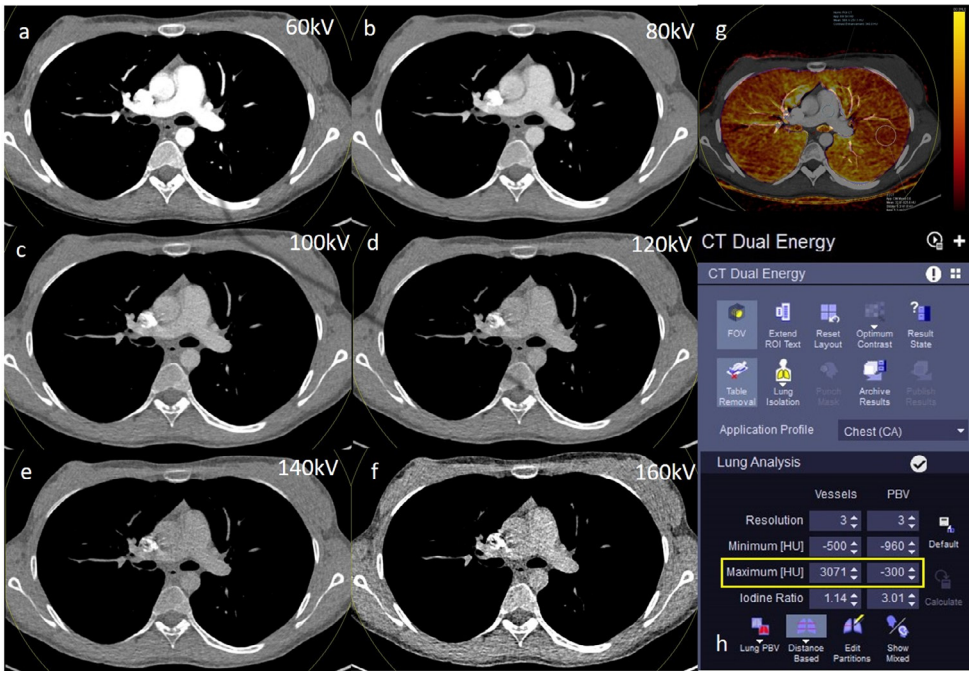

Figure 2 CTA of an 18-year-old female. (a-f) Single axial CTA slice at multiple kilovoltages: (a) 60 kV, (b) 80 kv, (c) 100 kV, (d)120 kV, (e)140 kv, (f)160 kV. (g) Axial color iodine map with perfusion overlay onto a mixed image demonstrating normal PBV. The yellow circle in the periphery reflects the 32 mm FOV of the smaller 80 kV source. The ROI over the main pulmonary artery gives a mean HU of the 80 and 140 kV and the HU of the contrast only (340.0 HU). The ROI in the left lung is a random blood volume sampling. The HU related to iodine is 32.8, corresponding to an iodine density of 1.1 mg/ml or 8.6% of that of the main pulmonary artery. (h) Example PBV parameters ideal for a pediatric patient, emphasizing the lower minimum PBV threshold (box). (Color version of figure is available online.)

However, a dual source DECT scanner utilizes 3 material decomposition which can be selected for exam type, for example a contrast-enhanced CT of the lungs, the 3 dominant materials in a given voxel are iodine, soft tissue, and air. Specific to perfusion evaluation, the attenuation of iodine is twice that at 80 kV as it is at 140 kV, and therefore the contribution of iodine to each individual voxel can be determined and subtracted. This can yield a virtual noncontrast image which can be used to assess for material which may otherwise be confused for iodine, such as calcium. Alternatively, the iodine can be displayed independently or as an overlay image where a color map of iodine distribution is superimposed upon the corresponding CT slice. In thoracic imaging, the iodine maps are most commonly used for assessing pulmonary blood volume (PBV), detailed later.

Contrast media allows for creation of an iodine distribution map

The thoracic applications described herein rely on properly timed iodinated contrast. At our institution CT angiogram (CTA) is performed after the intravenous administration of a nonionic low-osmolar iodinated contrast agent (Iohexol, OmnipaqueTM, 350 mg/mL, GE Healthcare Inc.) at a 2 mL/kg dose, followed by a 1 mL/Kg bolus of normal saline with the use of a dual-head power injector (Medrad Inc, Indianola, PA). Injection rate was set considering the available intravenous access catheter and calculated to achieve an infusion duration between 10 and 20 seconds. A manually triggered bolus tracking technique is used in all cases with regions of interest in either the left atrium, ascending aorta, descending aorta, right atrium or main pulmonary artery based on the indication. For example, CTA of pulmonary arteries, we use a right ventricular region of interest and use a guideline of 200 HU without breath hold delay or 150 HU with breath hold delay.

Once acquired, the 80 kV and 140 kV source data can then be postprocessed on a separate work station utilizing proprietary software (Syngo Dynamics software, version 9.0, Siemens Healthcare, Forchheim, Germany).

Postprocessing pearls

PBV acts as a surrogate for pulmonary perfusion

PBV is the iodine distribution map, typically displayed as a color overlay. The color overlay is displayed as a scale of the concentration of iodine on a background of the mixed CT image (Fig. 2). The default PBV Hounsfield (HU) numbers for the postprocessing software are set for and adequate in generating the PBV of older children or adult lungs, but for younger patients the thresholds must be adjusted as a basic starting point to include all perfused lung.

The iodine contrast map must then be normalized to the pulmonary blood concentration. This is accomplished by using a region of interest marker on the main pulmonary artery. Then, the pulmonary artery enhancement can be compared to the concentration of iodine within the lung parenchyma. Now an accurate iodine color map overlay can be viewed and perfusion to lung can be qualified. The relative blood volumes can also be quantified for specific lung regions with absolute iodine concentration measured in mg/cm. By drawing regions of interest over varying areas of lung tissue one can compare the degree of perfusion in those regions. The lung can also be segmented in a variety of manners so that volumetric information of enhancement from each segment can be quantified in table format (Fig. 3). While true perfusion imaging would require imaging at multiple time frames, the blood volume acts as a surrogate marker. The perfusion map has been shown to be comparable to actual perfusion in pig models and to that of nuclear medicine perfusion studies, and the map should be interpreted in the same manner (Fig. 4).[5,8]

Virtual noncontrast monoenergetic images

With 2 discrete points available at both 80 and 140 kV, the data sets can be plotted on a graph and can be extrapolated to form images ranging from 40 to 190 kV. At the low (80 kV) setting, the detection of iodine increases, which allows for a reduction in contrast material volume.[9] However, the lower KeV that shows the highest iodine signal also results in a significant increase in image noise.[10]

The optimization of iodine detection is most commonly used for improving visualization of small blood vessels for example in pulmonary embolism (Fig. 5). Another common application for low monoenergetic images is to "salvage" studies with low amounts of iodine due to an inappropriately timed contrast bolus.[11,12] On the other end of the spectrum are virtual noncontrast images. This technique identifies pixels containing both water and iodine and subtracts the iodine to yield an image that gives the appearance of a precontrast scan, thus eliminating the need for a second radiation dose.[2] The best examples for this are seen in renal imaging to look for stones and brain images to look for hyperdense blood products, with limited usage to date in thoracic applications.

Metal artifact reduction

Similar to virtual noncontrast images, at the higher end of the spectrum, high kV can decrease the beam hardening caused by metallic hardware. In patients with metallic hardware, the metal results in artifact from beam-hardening and photon-starvation effects, degrading the quality of the images. These artifacts can degrade image quality, obscure visualization of adjacent structures and pathologic processes, and decrease the diagnostic value of the examination. Monoenergetic high kV images reduces the beam hardening causing metal artifact, increase signal to noise ratio and improve the overall quality of the images near the metal without increasing the radiation dose.[13,14] Moreover, metal artifact reduction by means of DECT can still be combined with other metal

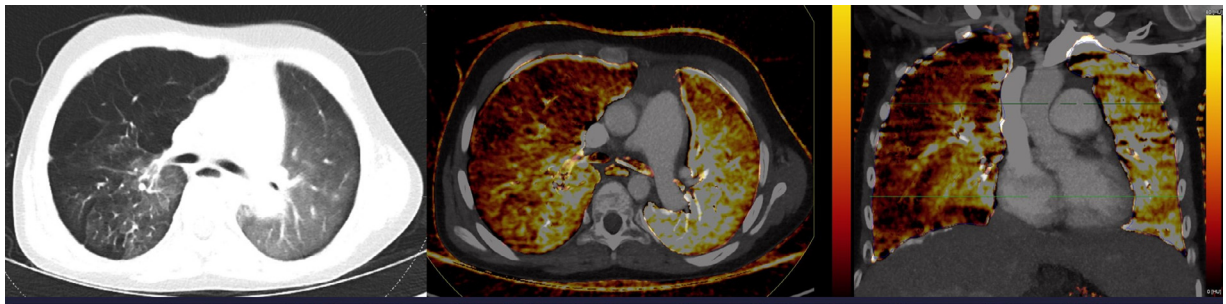

	Volume [cm3]	Full Volume [cm3]	Below Min [% of Voxels]	Above Max [% of Voxels]	Enhancement [HU]	Rel. Enhancement [%]
Total	2246	2246	11	2	42+/-36	94
Left and Right Lung						
Right	1487	1487	17	2	28+/-29	64
Left	760	760	0	4	63+/-35	143
Parts of Right Lung						
Right - Upper	344	344	33	0	22+/-28	50
Right - Middle	758	758	12	2	32+/-30	73
Right - Lower	385	385	14	1	25+/-27	57
Parts of Left Lung						
Left - Upper	193	193	0	3	61+/-42	139
Left - Middle	373	373	0	4	60+/-35	136
Left - Lower	194	194	0	5	72+/-28	163

Lung partitioning mode:	Distance Based
Minimum (Lung PBV):	-960 HU
Maximum (Lung PBV):	-300 HU
Measured Vessel Enhancement:	295 HU
Scaling:	0.15
	44 HU Corresponds to 100%

Figure 3 An 11-year-old male with congenital right diaphragmatic hernia status post repair. (a) Axial CTA in lung windows. Note the decreased attenuation and architectural distortion and hyperaeration of the right lung and relatively smaller left lung. (b) The iodine map at the same axial CT level demonstrating marked diminished perfusion to the hyperaerated right lung, particularly noticeable when compared to the normal left lung. (c) Coronal iodine map with segmentation. Two bilateral horizontal green lines dividing each lung into 3 segments are based on equal distances. The lungs are automatically outlined by the software, shown here as a blue line. (d) The segmentation tool allows for processing quantifiable perfusion data to each lung region. The first column shows the overall lung volume. The hyperinflated right lung is unsurprisingly larger than the left. The number of voxels below the minimum threshold value [Below Min] (set to −960) shows the poor perfusion of each right lung segment. This is also assessed in the enhancement and relative enhancement columns. Relative enhancement is determined by the scaling, set to 0.15, reflecting 15% of the main pulmonary artery value (Measured Vessel Enhancement: 295 HU). (Color version of figure is available online.)

reduction algorithms, allowing to further improve the image quality.[15]

In children, one of the common scenarios is the need to image cardiac or central vascular structures in postsurgical patients such as those with posterior spinal fusion hardware for scoliosis repair or those with vertical expandable prosthetic titanium ribs to evaluate for potential hardware failure (Fig. 6). Virtual monoenergetic images between 110 keV and 150 keV can significantly reduce metal artifact by preferentially removing the low-energy photons that result in beam hardening.[16] Another potential application in which minimizing metal artifact might play a crucial role, is the identification of impingement of the coronary arteries by epicardial leads.[17,18] However, so far, we have not had a documented positive case in our practice.

Contrast applications

PBV essentially evaluates the enhancement pattern of the lungs. However, the only validated use in pediatrics has been in pulmonary embolism. In adults PBV has been explored in the assessment of pulmonary hypertension.[19,20] and lung nodules.[21,22] Current and potential future applications in the pediatric patients are discussed in brief.

Pulmonary embolism

The most common cardiothoracic application of DECT perfusion is the evaluation of pulmonary embolism. Both larger segmental defects and smaller subsegmental defects may be observed, appearing as wedge shaped areas of absent perfusion (Fig. 5). Patients with nonocclusive PE may not demonstrate perfusion defects (Fig. 5h and i). This information increases diagnostic certainty about the presence of thrombus, improves the detection of small, peripheral emboli and evaluates the hemodynamic importance of nonocclusive and small emboli, which may be of minor relevance.

Hypoplastic lung

A hypoplastic lung will be hyperlucent and oligemic, regardless of cause. This is well seen on perfusion

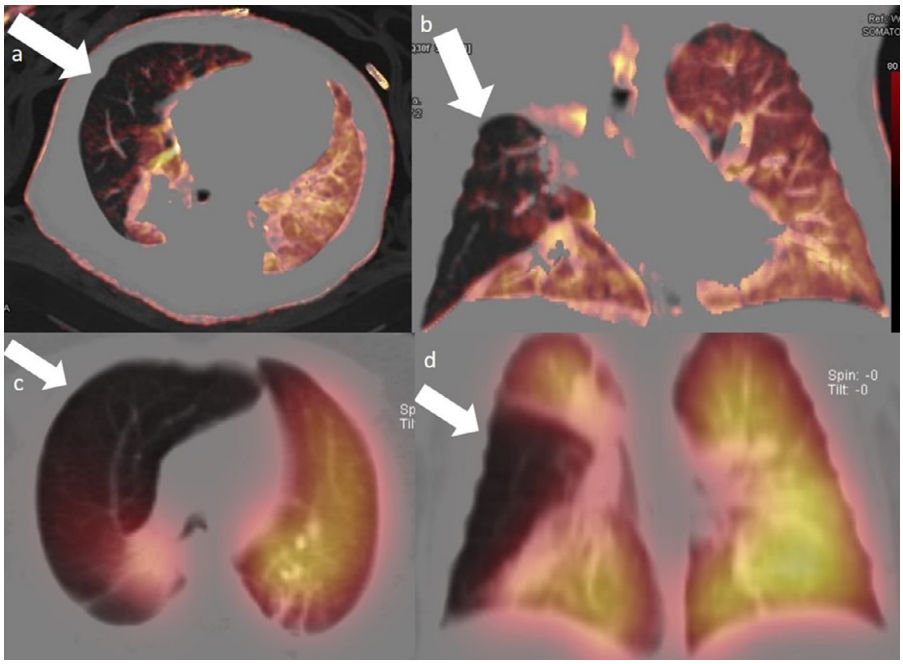

Figure 4 A 3-month-old male with right middle lobe congenital lobar overinflation (CLO). (a, b) Axial and coronal pulmonary blood volume images displayed as a color overlay. Not the marked regional decreased perfusion of the right middle lobe (arrows). (c, d) Representative fused axial and coronal SPECT/CT nuclear medicine perfusion study at 6 months of age. Note the similarities of the underperfusion of the right middle lobe (arrows). (Color version of figure is available online.)

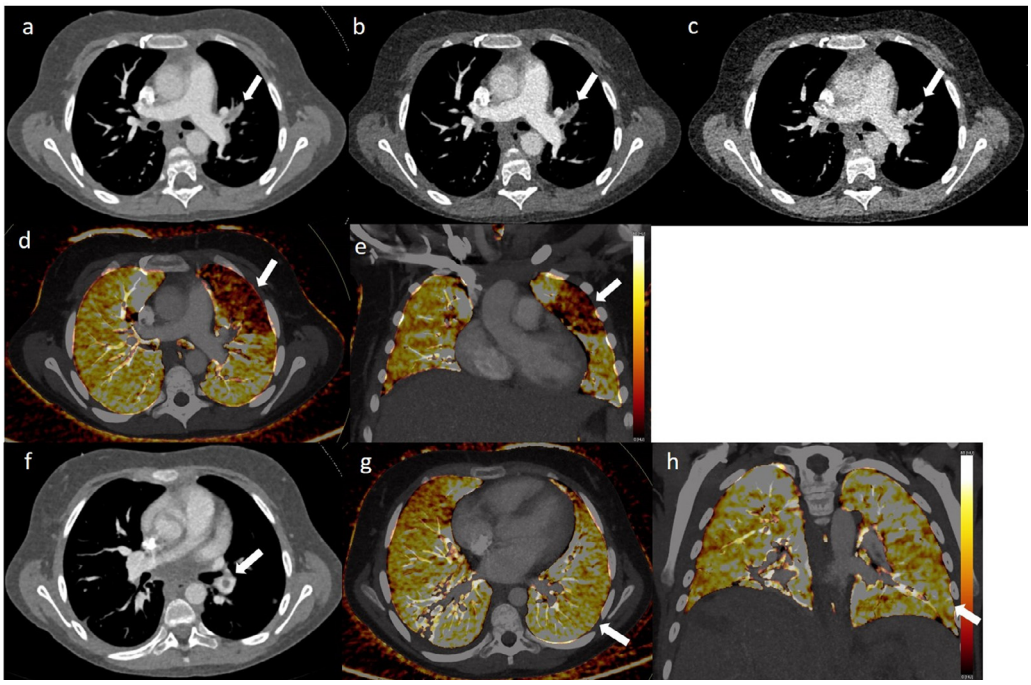

Figure 5 Ten-year-old female. (a) A composite mixed image with a 0.60 ratio (60% 80 kv and 40% 140 kv). Note the left upper lobar artery occlusive PE (arrow). The left upper lobar artery occlusive PE is much more easily appreciated on the 80 kv (b) than the 140 kv (c) source image due to the greater attenuation of iodine at the lower energy level. Axial (d) and Coronal (e) images of the iodine color overlay on a mixed image of the same patient. Note the large area of perfusion defect comprising the majority of the left upper lobe corresponding with the location of the PE. The left-sided color legend is derived from the HU contribution of each voxel by iodine. (f) The same patient with a nonocclusive PE in a left lower lobar artery on mixed image. Axial (g) and coronal (h) color iodine overlay does not demonstrate perfusion defects in the left lower lobe downstream from the nonocclusive PE. (Color version of figure is available online.)

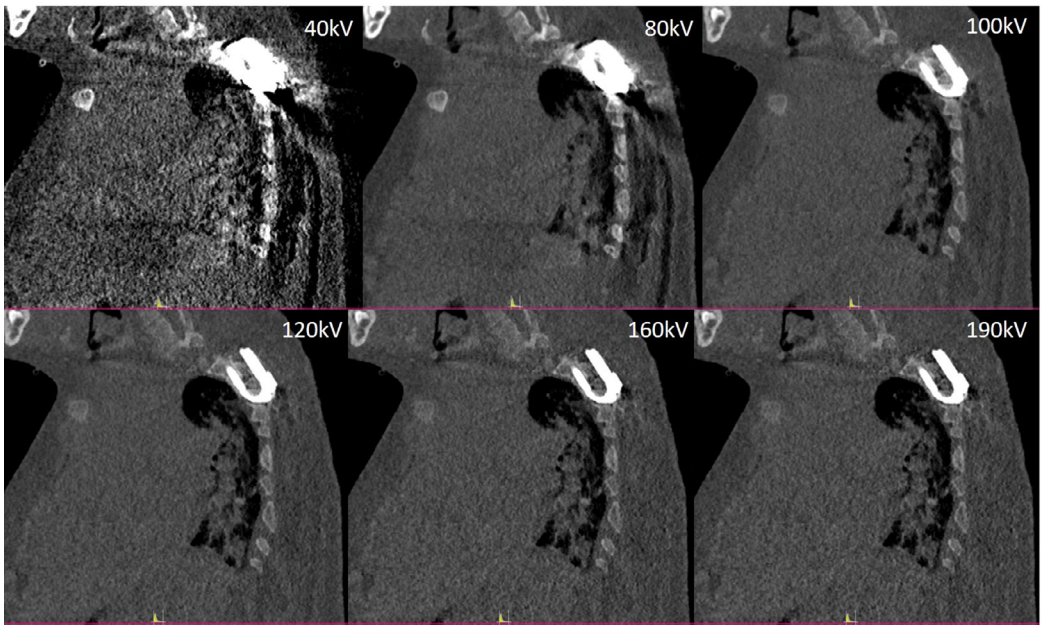

Figure 6 Patient with VEPTR devices. Images focused on the superior hook are shown in sagittal ranging from 40 kV (a) to 190 kV (f). With higher kV there is improved definition of the hardware and decreased streak artifact, though higher than 160 kV there is diminished improvement in artifact.

imaging as a diffuse decrease in PBV to the affected lung (Fig. 3). With DECT-perfusion, the lung can be segmented in order to qualify and quantify which lobes are most affected, equivalent to nuclear medicine V:Q scans. This provides valuable clinical information to clinicians as to quantify the degree of underperfusion, which might guide interventions based on if the dominant abnormality is inadequate vascular supply, airway stenosis or parenchymal disease. Relative perfusion can also be quantified in a tabled format (Fig. 3d). The resulting perfusion map is similar to that seen for nuclear medicine perfusion studies demonstrating lobar, segmental, or subsegmental perfusion defects in a way that is familiar to anyone who has interpreted the perfusion portion of a V:Q scan (Fig. 4).

Pulmonary hypertension in bronchopulmonary dysplasia

Neonates and infants with bronchopulmonary dysplasia commonly undergo CTA to evaluate for pulmonary hypertension. In severe bronchopulmonary dysplasia, heterogenous perfusion abnormalities are seen throughout the lungs (Fig. 7). The most challenging feature with these patients is the dense nature of the infant lung and the inability of commercial software to accurately record and tabulate perfusion in these regions. More work in this area is needed with the expectation that the identification of different perfusion abnormalities patterns might have prognostic value in this group value as those with poorer perfusion are likely at higher risk for long term ventilation dependence.

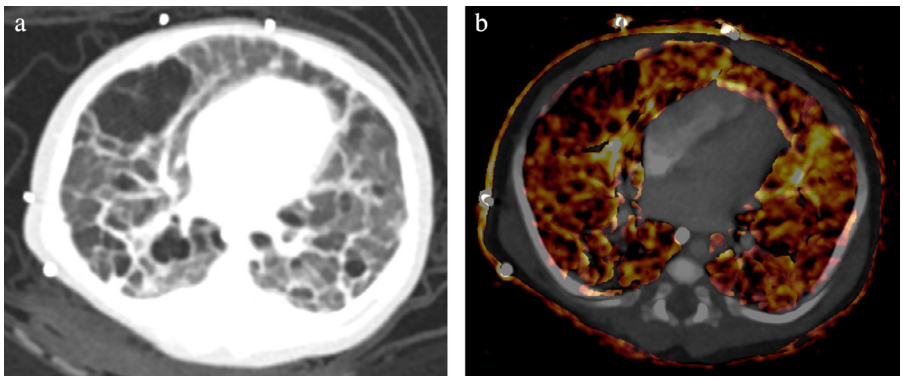

Figure 7 A 3-month-old male with bronchopulmonary dysplasia and hypertension. (a) Axial CTA mixed image through the lower lung zones. Note the marked heterogeneity of the lungs with cystic changes and air trapping. (b) The color map overlay at the same lung region demonstrates the corresponding heterogenous perfusion to the dysplastic lung tissue. (Color version of figure is available online.)

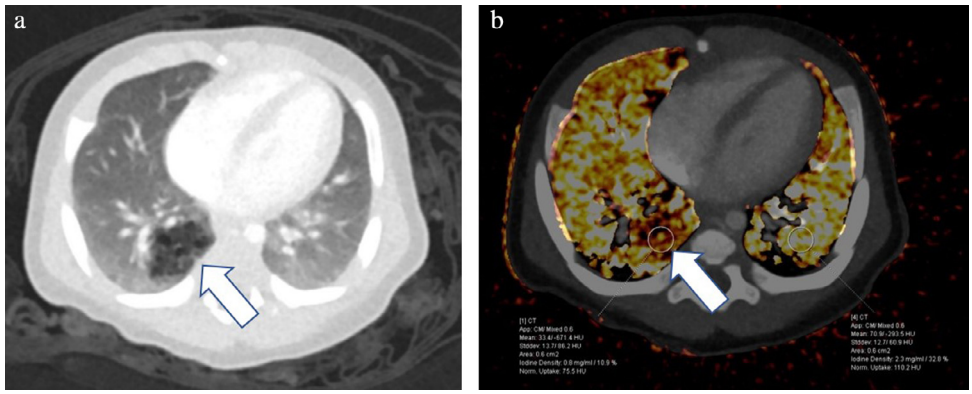

Figure 8 Two-month-old male. Cystic appearing right lower lobe lesions (arrow) is seen on the axial CTA in lung windows (a). The iodine map overlay (b) demonstrates focal decreased perfusion to this region with an iodine concentration of 0.8 mg/ml, compared to 2.3 mg/ml of normal left lower lobe lung parenchyma. This was surgically confirmed to represent a CPAM.

Pediatric lung masses

Pediatric lung masses can be evaluated in a similar manner as described. The degree of perfusion to lung lesions has been described in the adult literature in evaluation of pulmonary nodules.[21] This can be extrapolated to uniquely pediatric lung lesions. Perfusion software allows one to exclude a non-contrast study and still determine the degree of enhancement of a lesion. This may help differentiate a congenital pulmonary airway malformation (Fig. 8) from a bronchopulmonary sequestration from a hybrid lesion. The degree of contrast enhancement will also differentiate pulmonary vs systemic enhancement depending on bolus timing.

Technique and postprocessing pitfalls

Contrast bolus streak artifact

A common pitfall is due to dense contrast arriving through the subclavian veins or SVC and resulting in streak artifact that will artificially raise the iodine contribution to the HU of the adjacent upper lung (hence overestimating perfusion) (Fig. 9). This can be avoided by (i) optimizing the contrast timing and the saline bolus chaser, (ii) using a lower concentration of contrast mixed with saline at the tail end of the bolus, (iii) using less contrast or a lower concentration contrast agent, and/or (iv) using a foot injection, because streak from the inferior vena cava is less likely and produces less artifact. Pulsation from the heart and breathing motion can also result in artifact, especially in younger patients with faster heart and respiratory rates, but usually not as relevant for the perfusion calculation.

Dense lung parenchyma

Another common pitfall often encountered in the very young child is atelectasis. Collapsed lung tissue or consolidated lung is often too dense to be initially recognized

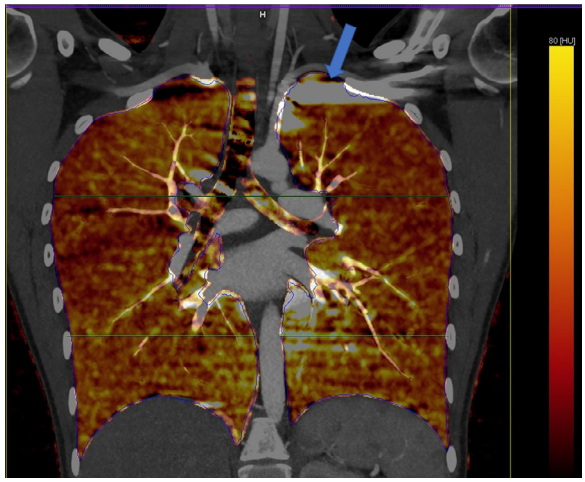

Figure 9 Coronal color map of the same patient in Fig. 2. Note the lung segmentation into 3 sections in each lung (green lines). The contrast bolus in the left subclavian vein results in significant streak artifact and artificially elevating the iodine density of the adjacent left apex (arrow). (Color version of figure is available online.)

by the software, artifactually underestimating the amount of parenchyma that is normally perfused.[23] It is possible to adjust the upper HU threshold manually and attempt to include the denser soft tissue. The minimum HU is by default set for −960, and everything which has a lower value will be excluded from evaluation. The maximum value is general defaulted to −600 for adult lungs, but should be adjusted to at least −300 HU in order to include the denser neonatal and infant lung.[5] If there are significant areas of ground glass opacities or atelectasis, this maximum number can be increased further to include these regions, as they are adequately perfused though are not ventilated. However, the software may still not recognize the border of the lung fields in the denser lung segment, potentially precluding the incorporation of the tissue into the perfusion evaluation and obtaining an accurate measurement of perfused lung.

Small field of view

The field of view (FOV) for the lower kV detector is smaller at 32 cm, while the higher kV detector is 50 cm. This results in decreased signal from the periphery of the image, which will be denoted on the mixed image as a circle at the 32 cm mark (Fig. 2). This result in a lack of a composite image for all tissue outside of the 32 cm FOV and therefore no ability to utilize material decomposition, during post processing on excluded tissue. Fortunately, for the majority of pediatric patients, most or all tissue will fall within the 32 cm low kV window, and typically the tissue that may fall outside the inner 32 cm ring will be subcutaneous fat, permitting evaluation of the entirety of the lung fields.

Motion

A single source scanner with temporal acquisitions is ill suited for the pediatric patient susceptible to motion. In larger patients, the low kV FOV may result in excluded lung tissue, resulting in nonevaluable lung parenchyma. Although this might only be a problem with adolescent and young adults, and with older generation models with only a 26 cm FOV capability, it is important to be aware of the size limitation while planning the study.

Dose

Radiation dose is considerably less than when compared to a dual phased study as DECT mitigates the need for a noncontrast phase. However, while DECT has been shown to be dose neutral in the head and abdomen, there is a slight dose penalty in the chest.[6] As Zhu et al showed in a phantom study that when compared to the optimized low dose study, there is a 20% and 11% increase in CTDIvol for 1-year-old and 5-year-old phantoms, respectively when contrast to noise ratio was preserved. There was no dose penalty, however, for 10-year-old phantoms. The DECT effective CTDIvol for these age groups were 0.78 mGy, 0.72 mGy, and 1.01 mGy in the 1, 5, and 10-year-old phantoms, respectively. These dosages remain well below the recommended upper limits in each age group (24) and therefore the small dose penalty may be acceptable if functional information can be obtained.

Conclusion

As the role of dual-energy CT continues to evolve, DECT-based perfusion adds functional information to an otherwise static CT scan, often at a neutral or reduced radiation dose. The newly found functional information have the potential to be of prognostic value in a variety of pediatric diseases including, but not limited to, pulmonary embolism, pulmonary hypertension, congenital vascular anomalies and the evaluation of lung lesions.

Funding source

No external funding for this manuscript.

Financial disclosure

The authors have indicated they have no financial relationships relevant to this article to disclose.

Conflict of interest

The authors have indicated they have no potential conflicts of interest to disclose.

References

1. Kalisz K, Halliburton S, Abbara S, et al: Update on cardiovascular applications of multienergy CT. Radiographics 37:1955-1974, 2017
2. Machida H, Tanaka I, Fukui R, et al: Dual-energy spectral CT: Various clinical vascular applications. RadioGraphics [Internet] 36:1215-1232, 2016. Available from: http://pubs.rsna.org/doi/10.1148/rg.2016150185
3. Yeh BM, Shepherd JA, Wang ZJ: Dual-energy and low-kVp CT in the abdomen. Am J Roentgenol 193:47-54, 2009
4. Pessis E, Campagna R, Sverzut J-M, et al: Virtual monochromatic spectral imaging with fast kilovoltage switching: Reduction of metal artifacts at CT. RadioGraphics [Internet] 33:573-583, 2013.. Available from: http://pubs.rsna.org/doi/10.1148/rg.332125124
5. Goo HW: Initial experience of dual-energy lung perfusion CT using a dual-source CT system in children. Pediatr Radiol 40:1536-1544, 2010
6. Zhu X, Mccullough WP, Mecca P: Dual-energy compared to single-energy CT in pediatric imaging: A phantom study for DECT clinical guidance. Pediatr Radiol [Internet] 46:1671-1679, 2016.. Available from: http://dx.doi.org/10.1007/s00247-016-3668-x
7. Siegel MJ, Kaza RK, Bolus DN, et al: White paper of the society of computed body tomography and magnetic resonance on dual-energy CT, part 1: Technology and terminology. J Comput Assist Tomogr 40:841-845, 2016
8. Fuld MK, Halaweish AF, Haynes SE: Pulmonary perfused blood volume with dual-energy CT as surrogate for pulmonary perfusion assessed with dynamic multidetector CT. Radiology [Internet] 267:747-756, 2013. Available from: http://www.ncbi.nlm.nih.gov/pubmed/23192773
9. Delesalle MA, Pontana F, Duhamel A, et al: Spectral optimization of chest CT angiography with reduced iodine load: Experience in 80 patients evaluated with dual-source, dual-energy CT. Radiology 267:256-266, 2013
10. Sudarski S, Apfaltrer P, Nance JW, et al: Optimization of keV-settings in abdominal and lower extremity dual-source dual-energy CT angiography determined with virtual monoenergetic imaging. Eur J Radiol [Internet] 82:e574-e581, 2013. Available from: http://dx.doi.org/10.1016/j.ejrad.2013.04.040
11. Leithner D, Wichmann JL, Vogl TJ, et al: Virtual monoenergetic imaging and iodine perfusion maps improve diagnostic accuracy of dual-energy computed tomography pulmonary angiography with suboptimal contrast attenuation. Invest Radiol 52:659-665, 2017
12. D'Angelo T, Cicero G, Mazziotti S, et al: Dual energy computed tomography virtual monoenergetic imaging: Technique and clinical applications. Br J Radiol 92, 2019
13. Lee KYG, Cheng HMJ, Chu CY: Metal artifact reduction by monoenergetic extrapolation of dual-energy CT in patients with metallic implants. J Orthop Surg 27:1-7, 2019
14. Jagoda P, Schmitz D, Wagenpfeil S: Comparison of metal artifact reduction in dual- and single-source CT: A vertebral phantom study. Am J Roentgenol 211:1298-1305, 2018

15. Long Z, DeLone DR, Kotsenas AL, et al: Clinical assessment of metal artifact reduction methods in dual-energy CT examinations of instrumented spines. Am J Roentgenol 212:395-401, 2019
16. Hye JY, Hong SH, Chung BM, et al: Metal artifact reduction in virtual monoenergetic spectral dual-energy CT of patients with metallic orthopedic implants in the distal radius. Am J Roentgenol 211(November):1083-1091, 2018
17. Mah DY, Praskash A, Porras D: Coronary artery compression from epicardial leads: More common than we think. Circulation [Internet] 15:1792-1794, 2018. Available from: https://doi.org/10.1016/j.hrthm.2018.06.038
18. MacIcek SL, Cannon BC, Kyle WB: Dynamic coronary artery compression by pacemaker lead. Circulation 124:1792-1794, 2011
19. Ameli-renani S, Rahman F, Nair A, , et al. Dual-energy CT for imaging of pulmonary hypertension : RadioGraphics. 2014;34:1770−90.
20. Ameli-renani S, Ramsay L, Bacon JL, et al: Dual-energy computed tomography in the assessment of vascular and parenchymal enhancement in suspected pulmonary hypertension. J Thorac Imaging 29:98-106, 2014
21. Sudarski S, Hagelstein C, Weis M: Dual-energy snap-shot perfusion CT in suspect pulmonary nodules and masses and for lung cancer staging. Eur J Radiol [Internet] 84:2393-2400, 2015.. Available from: http://dx.doi.org/10.1016/j.ejrad.2015.09.024
22. Kang M-J, Park CM, Lee C-H: Dual-energy CT: Clinical applications in various pulmonary diseases. RadioGraphics [Internet] 30:685-698, 2010.. Available from: http://pubs.rsna.org/doi/10.1148/rg.303095101
23. Siegel MJ, Ramirez-Giraldo JC: Dual-energy CT in children: Imaging algorithms and clinical applications. Radiology [Internet] 291:286-297, 2019. Available from: http://pubs.rsna.org/doi/10.1148/radiol.2019182289
24. Strauss KJ, Goske MJ, Towbin AJ, et al: Pediatric chest CT diagnostic reference ranges: Development and application. Radiology [Internet] 284:219-227, 2017. Available from: http://pubs.rsna.org/doi/10.1148/radiol.2017161530